frontiers | Frontiers in Earth Science

TYPE Original Research
PUBLISHED 31 October 2025
DOI 10.3389/feart.2025.1642287

OPEN ACCESS

EDITED BY
Li Ang,
Jilin University, China

REVIEWED BY
Hongjian Zhu,
Yanshan University, China
Xin Li,
China National Offshore Oil Corporation, China
Victor Manuel Velasco Herrera,
National Autonomous University of Mexico, Mexico
Muhammad Tayyab Naseer,
Quaid-i-Azam University, Pakistan
Rusi Zuo,
Tongji University, China

*CORRESPONDENCE
Xingjian Wang,
wangxi@cdut.edu.cn

RECEIVED 06 June 2025
ACCEPTED 24 September 2025
PUBLISHED 31 October 2025

CITATION
Zhang Y, Wang X, Li Y, Jiang X and Zhang H (2025) Fracture prediction method and application based on multi-attribute fusion generative adversarial network. *Front. Earth Sci.* 13:1642287. doi: 10.3389/feart.2025.1642287

Fracture prediction method and application based on multi-attribute fusion generative adversarial network

Yongheng Zhang[1,2], Xingjian Wang[1,2]*, Yang Li[1,2], Xudong Jiang[2] and Han Zhang[1,2]

[1]State Key-Laboratory of Oil and Gas-Reservoir Geology and Exploitation, Chengdu University of Technology, Chengdu, China, [2]College of Geophysics, Chengdu University of Technology, Chengdu, China

In complex structural zones shaped by multi-phase tectonic movements, the coexistence of diverse structural origins and intricate hydrocarbon accumulation conditions makes fracture prediction a critical technical challenge in oil and gas exploration. Current methods face two key limitations: conventional single-attribute seismic analysis falls short of satisfying high-precision fracture detection requirements, while deep learning approaches, despite their progress, suffer from poor generalization due to limited training samples. To address these issues, this study proposes a multi-attribute fusion method that synergistically combines Wasserstein GAN (WGAN) and U-Net++. The proposed approach effectively enlarges the training dataset while maintaining geological fidelity, empowering the trained network to hierarchically extract fracture features across multiple scales. Field tests show our method achieves precise alignment with well-log interpretations and delivers superior performance to conventional attribute-based techniques in both major and micro-fracture identification, demonstrating superior noise resistance and generalizability for fracture prediction across different study areas.

KEYWORDS

multi-attribute calculations, generate adversarial network, U-Net++, fault characterization, dataset

1 Introduction

With accelerating development of the global economy, energy demand—particularly for natural gas and crude oil—has surged significantly. Conventional hydrocarbon resources are increasingly inadequate to meet evolving economic requirements, while persistent international price escalation has rendered unconventional oil and gas exploration an imperative research priority. Reservoir fracture systems, functioning as vital conduits and storage spaces for hydrocarbon migration and accumulation, remain central to petroleum geology and geophysical research. As exploration shifts toward deep, ultra-deep, and unconventional reservoirs, fracture prediction technology faces unprecedented challenges and opportunities. This study systematically investigates a hybrid multi-attribute deep learning framework based on generative adversarial networks (GANs), offering innovative solutions to address key scientific challenges in contemporary fracture characterization.

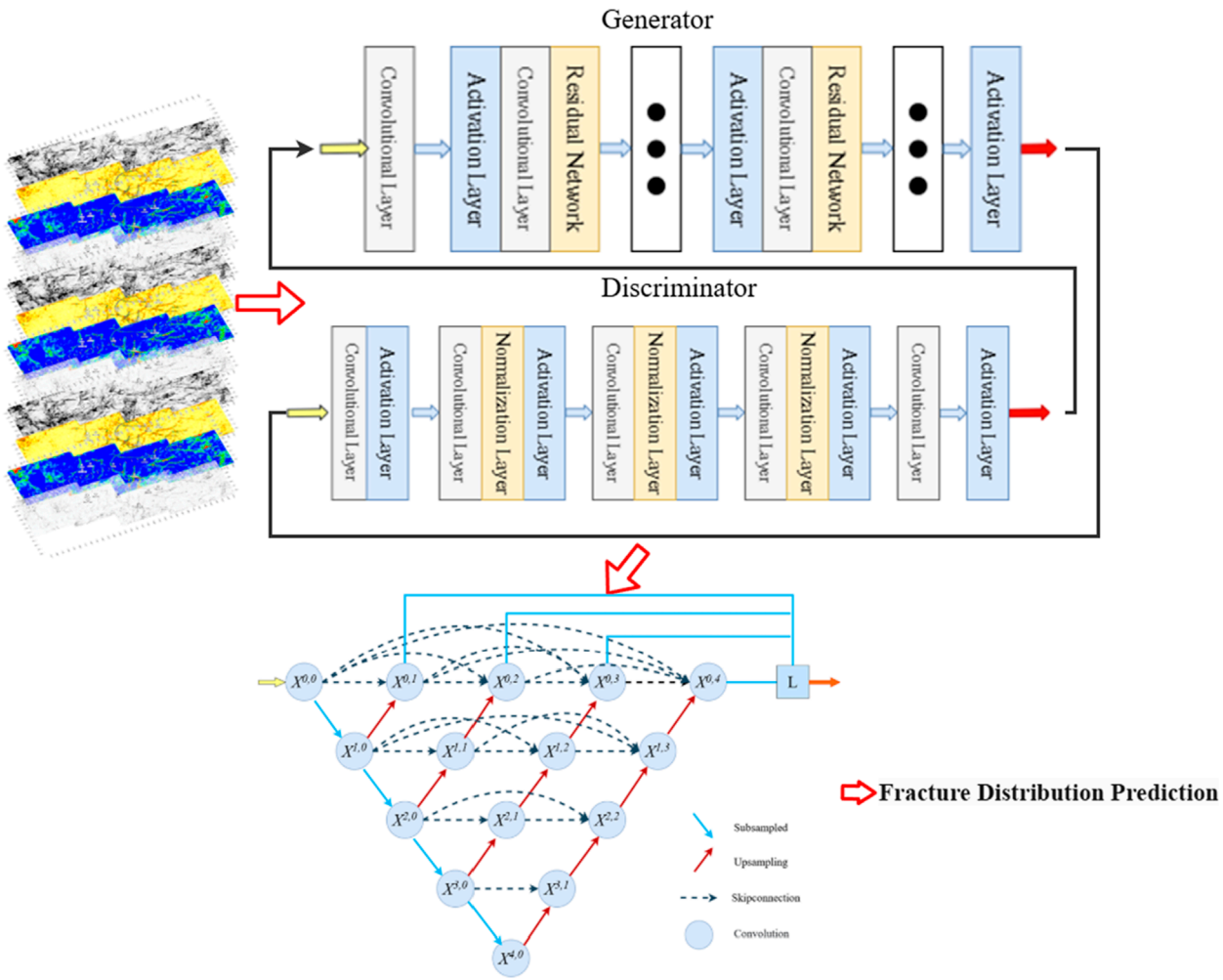

FIGURE 1
Multi-attribute fusion generative adversarial network flowchart.

With the advancement of signal processing technology, spectral analysis has emerged as an important supplementary approach in fracture prediction as a nonlinear method for extracting implicit frequency characteristics from seismic data. In recent years, significant progress has been made in the application research of spectral analysis for fracture prediction (Lei et al., 2024; Marfurt et al., 1998) by uncovering the implicit frequency-domain information in seismic data, spectral analysis provides a novel perspective for fracture prediction that differs from traditional geometric attributes, demonstrating strong adaptability particularly in weak signal zones or complex reservoirs (Cai et al., 2022). With the refinement of spectral decomposition techniques (such as improved time-frequency resolution), deeper understanding of absorption-attenuation mechanisms, (Sun et al., 2024) and the integration of artificial intelligence methods, spectral analysis is expected to become an indispensable technical approach for fracture prediction in the future, providing critical support for detailed reservoir characterization and efficient hydrocarbon development (Fu et al., 2024; Yuan et al., 2024).

Advancements in computational technologies have significantly propelled innovation in fault detection methodologies (Bi and Wu, 2021). Traditional approaches typically involve linking discontinuities in 2D seismic reflection horizons to construct fault frameworks. Established techniques encompass coherence cube analysis, variance analysis, edge detection (Dorigo et al., 1999), post-stack target processing, and forward modeling. The core fault identification technologies include coherence cube/volume analysis, variance cube analysis, ant colony optimization algorithms, and edge detection methodologies (Höcker and Fehmers, 2002; Zhou et al., 2022). These approaches provide critical guidance for fault interpretation with broad applicability, necessitating rigorous methodological selection during practical implementations to maximize positional accuracy. Ongoing technological progress continues to transform fault identification practices (Chopra and Marfurt, 2007). The synergistic integration of computer science and seismological expertise enables enhanced characterization of subsurface fault geometries (Gersztenkorn and Marfurt, 2002), offering crucial support for geological exploration and resource development (Kingma and Ba, 2014). These

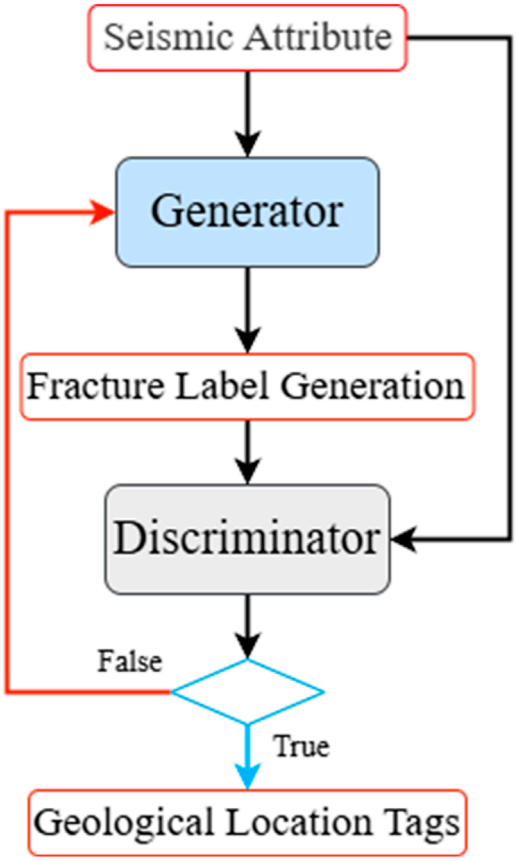

FIGURE 2
Architecture diagram of generative adversarial networks.

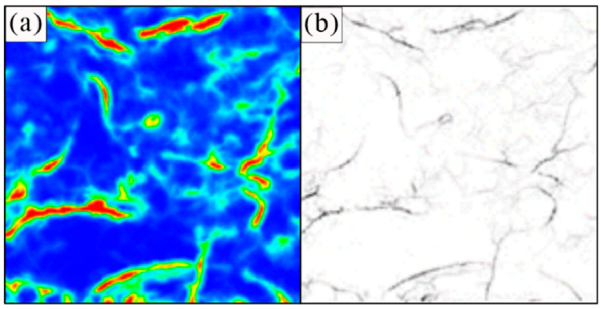

FIGURE 3
Fracture prediction results: Maximum likelihood Attribute **(a)** and refined maximum likelihood attribute **(b)**.

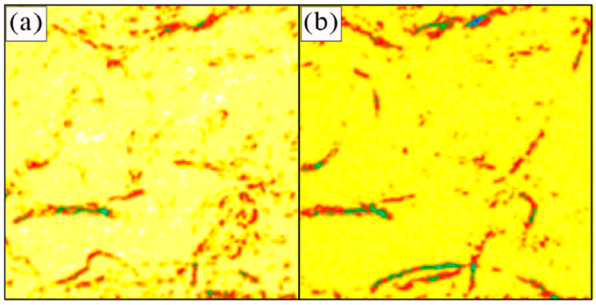

FIGURE 4
(a,b) Gradient structure tensor attribute prediction results.

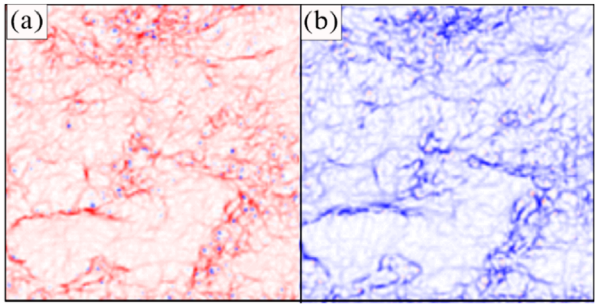

FIGURE 5
Maximum positive curvature attribute **(a)** and minimum negative curvature attribute fracture prediction results **(b)**.

Future advancements promise transformative breakthroughs in this domain.

The integration of machine learning technology has ushered in a new era of development. The inaugural application of backpropagation neural networks (BP) to multi-attribute fracture prediction significantly improved objectivity Subsequent adoption of support vector machines (SVM) and random forests nevertheless encountered inherent limitations due to shallow learning architectures' constrained representational capacity for complex fracture systems (Gibson et al., 2003) 2013–Present: Deep Learning Revolution (Cui et al., 2025). The transformative deployment of convolutional neural networks (CNNs) achieved breakthroughs in North Sea oil field fault identification (Wang et al., 2024). Generative adversarial networks (GANs) subsequently addressed small-sample learning challenges (Marfurt et al., 1998). Architectural innovations like U-Net and Transformer models ushered in intelligent fracture recognition (Bhunia et al., 2018). Recent advancements including 2.5D Transformer U-Net and Fault-Seg-Net demonstrate significant advantages in complex fracture scenarios (Chan et al., 2022; Xue et al., 2016). Notwithstanding progress, deep learning confronts critical data scarcity constraints: reliable fracture labels constitute <5% of total project data (Cao et al., 2024; Liu et al., 2025). Conventional augmentation strategies (rotational/flipping transformations) inadequately simulate complex fracture geometries, impairing model generalization—a particularly acute challenge in frontier basins with limited historical datasets (Ledig et al., 2017; Zhang et al., 2025).

As a data-driven paradigm, deep learning offers automation advantages and scalability. Modern machine/deep learning frameworks enable automated feature extraction and optimization (Lecun et al., 1998), achieving cross-industry adoption. This study proposes an enhanced hybrid multi-attribute deep learning framework that innovatively combines conventional attribute prediction methodologies (Bhunia et al., 2018). The system aims to improve exploration efficiency, optimize drilling success rates

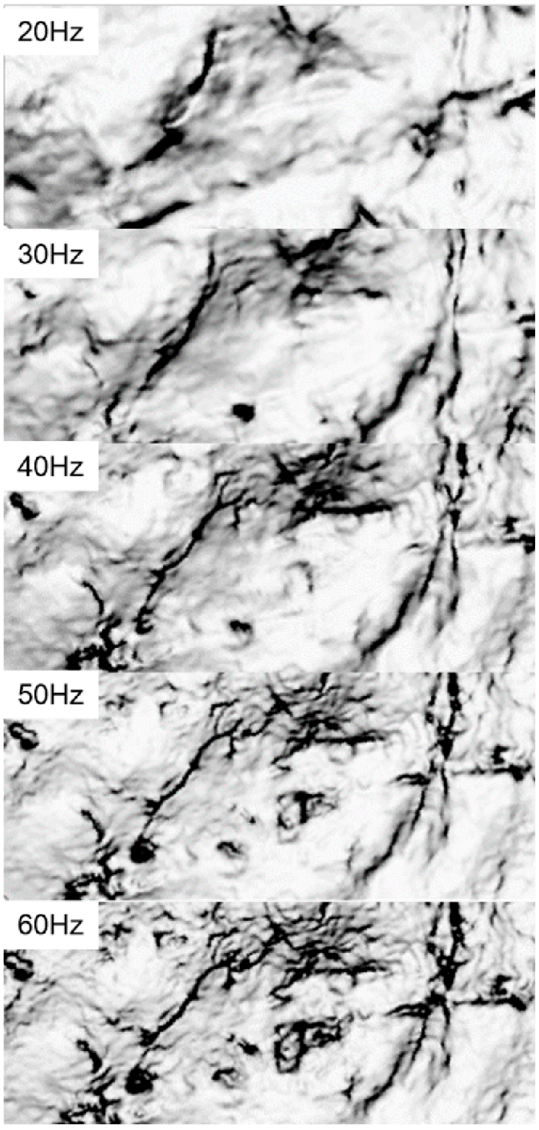

FIGURE 6
Fracture prediction results derived from frequency-dependent coherent attribute analysis under different frequency bands.

through subsurface engineering data integration, and investigate GAN-CNN synergies in fault identification while evaluating geological science implications (Di et al., 2019).

2 Methods

2.1 Workflow

This study introduces a deep learning architecture that integrates the Wasserstein Generative Adversarial Network (WGAN) and U-Net++, constructing a multi-attribute fusion-based fracture identification system (as shown in Figure 1) (Li et al., 2024). The single-attribute fracture prediction results from actual field data—including maximum likelihood attributes, coherent attributes, gradient structure tensor attributes, and curvature attributes—are fed into the WGAN (Xu et al., 2024). This ensures that the generated synthetic data exhibits geological plausibility while addressing the issue of scarce labeled data. The outputs from the WGAN are then processed by the U-Net++ network. The high-fidelity synthetic data substantially improves the realism and generalization capability during U-Net++ training. Once the network reaches stability (Gan et al., 2025), it is applied to reprocess the actual field data for fracture identification (Niu et al., 2024). The resulting predictions align more closely with manual interpretations and demonstrate markedly enhanced performance in detecting small-scale fractures (Ding et al., 2025; Chopra and Marfurt, 2007).

2.2 Label generation using multi-attribute fusion generative adversarial network

2.2.1 Wasserstein Generative Adversarial Network (WGAN)

Goodfellow et al. proposed a novel architecture based on convolutional neural networks in 2014, which introduced a fundamental departure from traditional neural networks by comprising two components: a generator and a discriminator. This framework was named Generative Adversarial Networks (GAN) (Wu et al., 2021).

As illustrated in Figure 2 the input data includes "ingredients" required to synthesize realistic data: original feature values (labels), random noise, and raw data. Through the generator, new labeled data is produced and passes the discriminator's evaluation. After iterative training, the network ultimately generates data indistinguishable from real samples (Mao et al., 2017).

Traditional GANs employ KL divergence or JS divergence for training, but these methods suffer from issues like gradient vanishing and mode collapse. To address these problems, the Wasserstein Generative Adversarial Network (WGAN) was proposed. The core innovation of WGAN lies in replacing traditional divergence metrics with the Wasserstein distance to measure the distance between probability distributions (Equation 1).

$$W\left(P_r, P_g\right) = \inf_{\gamma \sim \prod\left(P_r, P_g\right)} E_{(x,y)\sim\gamma}[\| x - y \|] \tag{1}$$

In the above formula, $\prod\left(P_r, P_g\right)$ represents the set of all joint distributions of P_r and P_g. For each possible joint distribution γ,the distance $\| x - y \|$ between the real sample x and the fake sample y can be calculated. Then, the expected value $E_{(x,y)\sim\gamma}[\| x - y \|]$ of the samples and the distance for the joint distribution γ can be computed. The lower bound $\inf_{\gamma \sim \prod\left(P_r, P_g\right)} E_{(x,y)\sim\gamma}[\| x - y \|]$ of the entire probability is the Wasserstein distance. It can be understood that $E_{(x,y)\sim\gamma}[\| x - y \|]$ represents the energy consumption required to push P_r to P_g under the overall situation of γ and $W\left(P_r, P_g\right)$ is the minimum consumption for the shortest distance.

Since the solution of $\inf_{\gamma \sim \prod\left(P_r, P_g\right)}$ cannot be obtained directly, it is changed to a Lipschitz - continuous form. That is, a restriction condition is added to the function to obtain an optimal solution that can be used as a substitute. As shown in Formula 2.

$$W\left(P_r, P_g\right) = \frac{1}{K} \sup_{\|f\|_L \le K} E_{x\sim P_r}[f(x)] - E_{x\sim P_g}[f(x)] \tag{2}$$

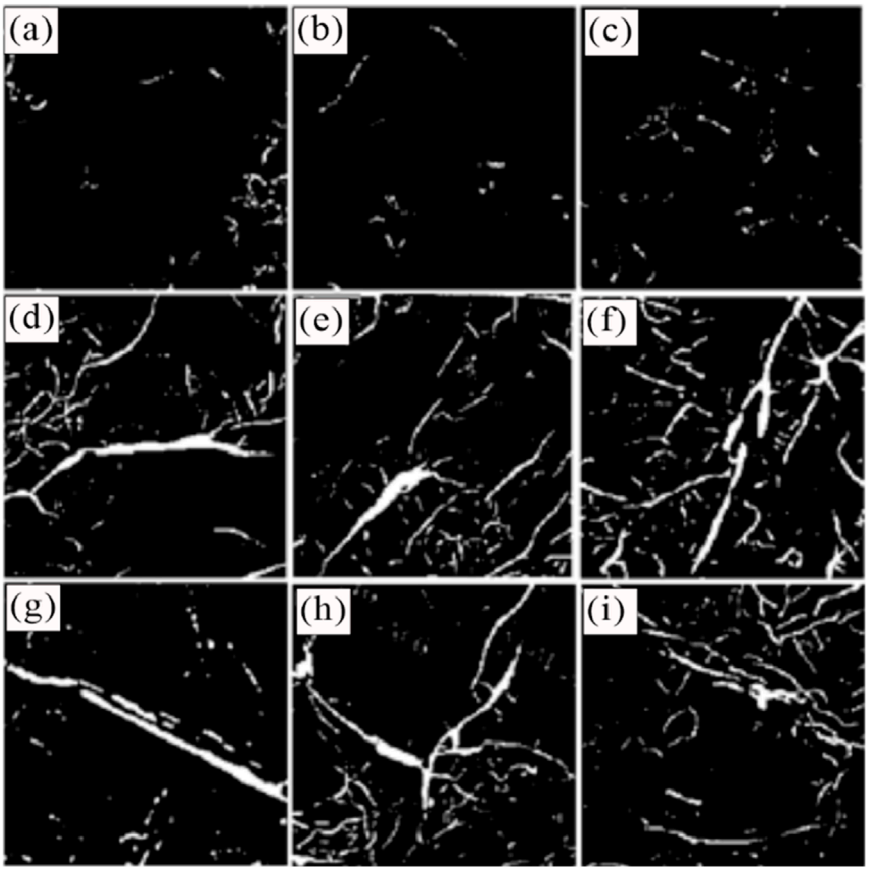

FIGURE 7
Augmented Labeled Dataset via WGAN Network **(a–c)**:Labels generated from iterations 50 **(d–i)**:Labels generated after network stabilization.

In the above - mentioned (Formula 3), $K \geq 0$ and any two elements must satisfy.

$$|f(x_1) - f(x_2)| \leq K|x_1 - x_2| \tag{3}$$

which is indicated by the arrow (3). K is called the Lipschitz constant. Then, Formula 5 can be understood as taking the upper bound of $E_{x\sim P_r}[f(x)] - E_{x\sim P_g}[f(x)]$ for all eligible under the condition of the constant K,and then shrinking it by K times. In generative adversarial networks, the parameter ω is needed to complete the update of the function $f(\omega)$, as shown in the following Formula 4.

$$K \cdot W\left(P_r, P_g\right) \approx \max_{\omega:|f_\omega|_L \leq K} E_{x\sim P_r}[f_\omega(x)] - E_{x\sim P_g}[f_\omega(x)] \tag{4}$$

$$L = E_{x\sim P_r}[f_\omega(x)] - E_{x\sim P_g}[f_\omega(x)] \tag{5}$$

The results obtained in the above formula are approximate to the Wasserstein distance between the real samples and the generated samples. By minimizing the Wasserstein distance, that is, minimizing L, the problem of gradient vanishing can be solved. Since the activation function in the last layer of the discriminator network in the original GAN is designed for a binary classification task, but now it is improved using the Wasserstein distance, there is no need to continue using the Sigmoid function as the activation function in the last layer. From Equations 6, 7, we can obtain the latest loss functions of the two networks.

$$L_G = -E_{x\sim P_g}[f_\omega(x)] \tag{6}$$

$$L_D = E_{x\sim P_r}[f_\omega(x)] - E_{x\sim P_g}[f_\omega(x)] \tag{7}$$

In summary, the key improvements of WGAN can be categorized into four principal aspects: (1) Removing the Sigmoid function in the last layer of the discriminator network; (2) Adopting the improved forms of the loss functions for both the generator and discriminator networks as mentioned above, instead of using the log - form; (3) Ensuring that the absolute value of the updated parameters does not exceed a fixed constant; (4) Selecting appropriate optimization algorithms. Sometimes, using momentum gradient descent and adaptive moment estimation algorithms may cause instability in the loss function, leading to substantial variations in the generated samples.

2.2.2 Label data preparation

The utilization of highly geologically plausible and high-fidelity labeled data can significantly enhance the predictive performance of neural networks. This study employs a WGAN (Wasserstein Generative Adversarial Network) to generate high-quality labeled data. The process first requires obtaining prediction results from

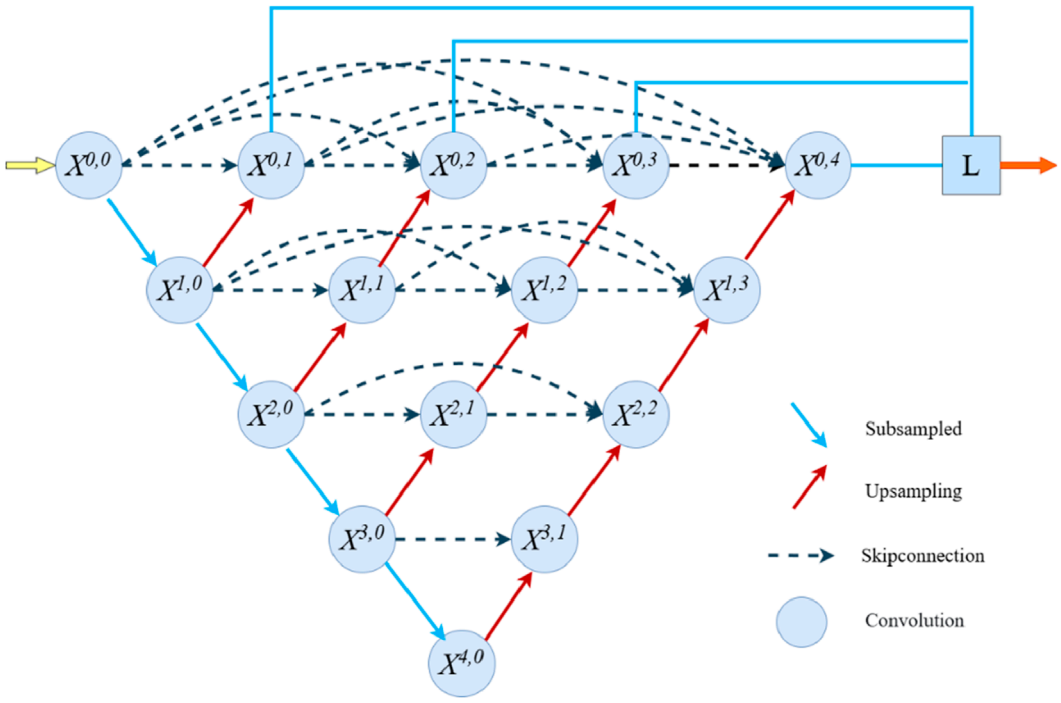

FIGURE 8
U-Net++ convolutional neural network architecture.

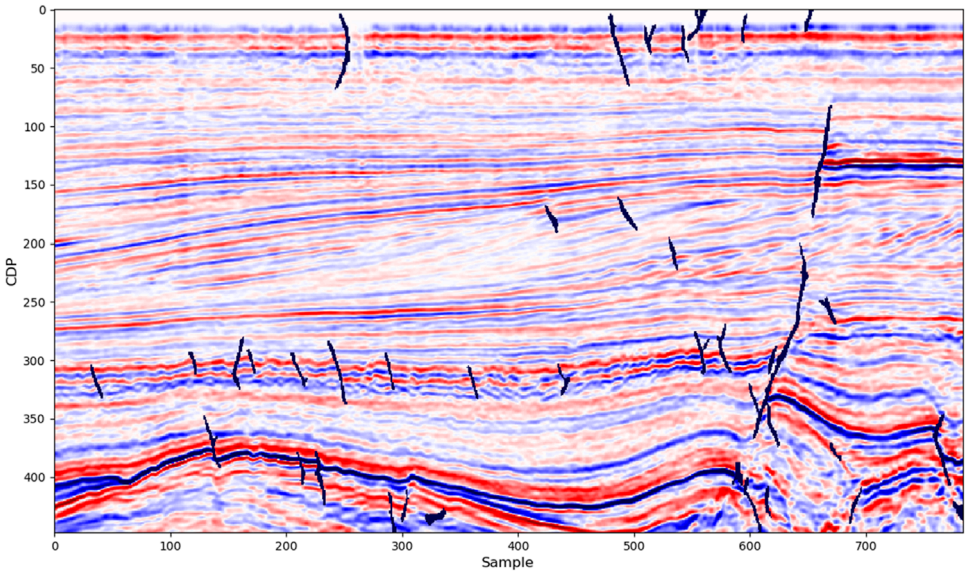

FIGURE 9
Fracture interpretation results manually identified by experts.

actual seismic data processed through single-attribute analysis within the target area, which serves as the "raw material" for training the WGAN. For validation purposes the North Sea F3 Block in the Netherlands, a publicly available seismic dataset collected in 1987, is widely referenced in studies on AI-based seismic fault detection. This dataset contains numerous faults with distinct characteristics, making it an excellent benchmark for validating the model's training effectiveness.

First, the seismic data is processed using the single-attribute method (Figures 3–6), and its prediction results are input into the WGAN network. Through multiple iterations, this generates labeled data that more closely resembles real geological samples.

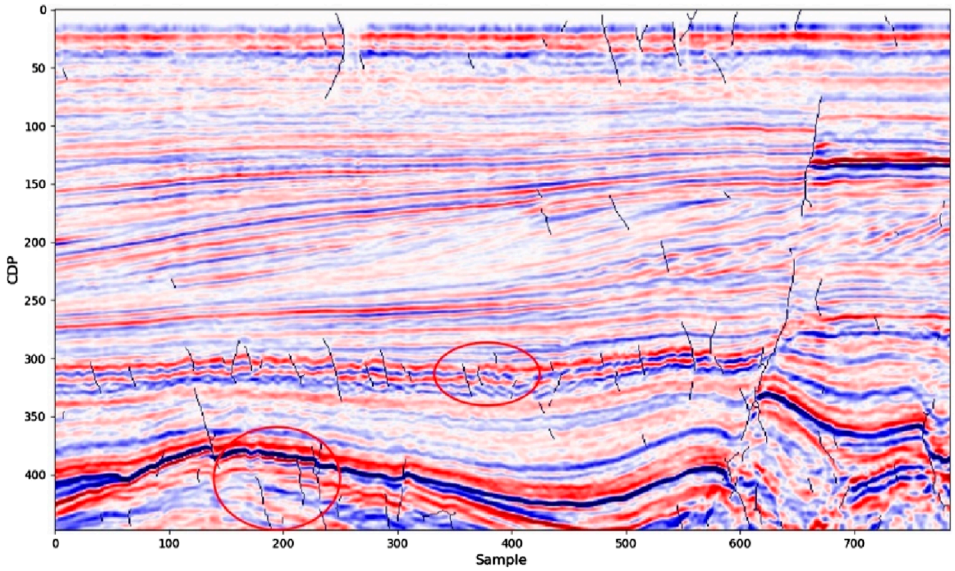

FIGURE 10
Fracture prediction results using manually labeled data.

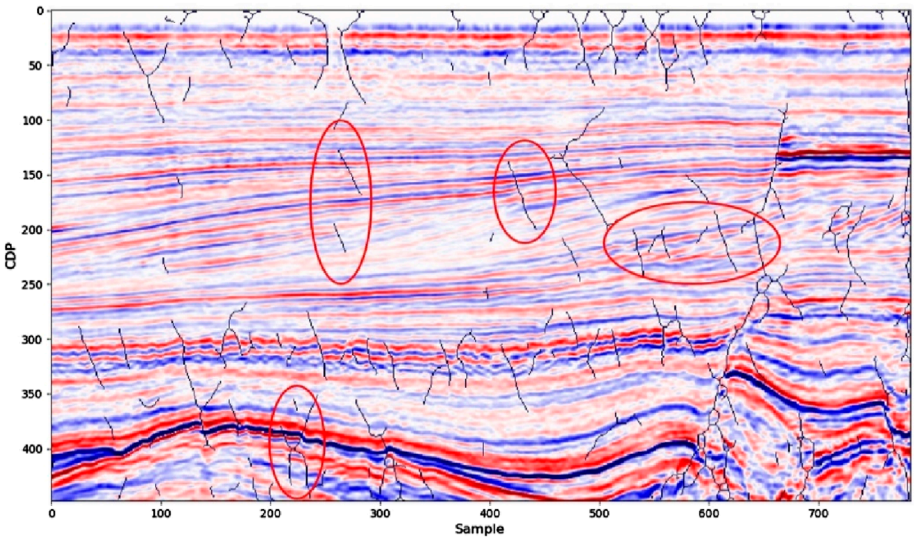

FIGURE 11
Fracture prediction results using labels generated by the multi-attribute fusion generative adversarial network.

After processing the single-attribute-generated results through slicing and grayscale/binary image processing, geologically realistic labeled samples are obtained. These pseudo-labeled samples are then input into the generator network. The generated pseudo-labeled data and real data are subsequently assessed for authenticity by the discriminator network. Through iterative refinement, the gap between the generator's output and the real data gradually diminishes until high-quality labeled data meeting research requirements is achieved, thereby completing the expansion of the labeled dataset.

The WGAN-generated label samples successfully mitigate the issue of sample scarcity in previous methods. As demonstrated in the figure below, which depicts label samples obtained from the trained network, the generated labels exhibit enhanced realism and diversity. Unlike prior approaches that were constrained to detecting only prominent fractures and simplistic/linear labels, these improved results demonstrate finer structural details and more natural variations, thereby achieving closely alignmen with real-world geological features (Figure 7).

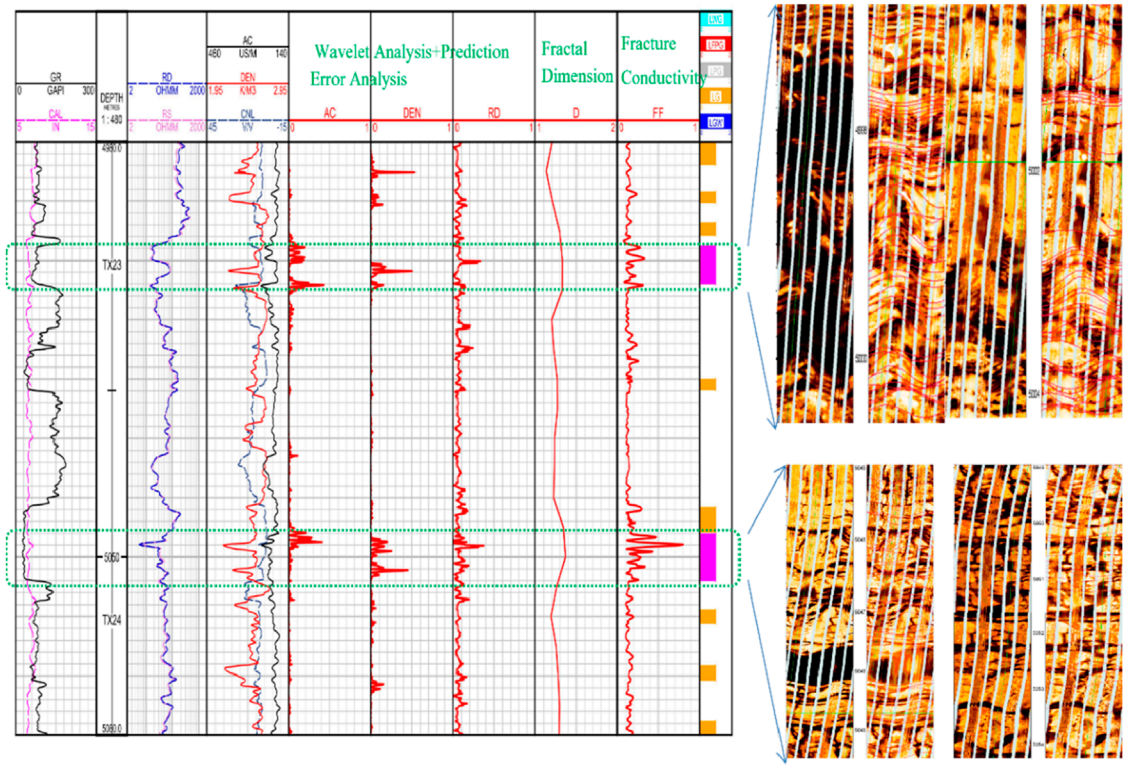

FIGURE 12
Comprehensive Fracture Evaluation of Well 1 vs. Imaging Well Logging-Based Fracture Development.

2.3 Fracture prediction network architecture

U-Net++ is an advanced segmentation model proposed in previous studies, first developed for medical image segmentation and conceptually extended from the U-Net architecture. It belongs to a deeply supervised "encoder-decoder" network structure. Building upon the U-Net convolutional neural network, it enhances the architecture through deeply supervised encoder-decoder mechanisms, with the specific structure illustrated in Figure 8 (Zhu et al., 2017). The U-Net++ network integrates sub-U-Net structures at different hierarchical levels and introduces dense connections and multi-scale feature fusion mechanisms into the original U-Net design (Xue et al., 2016). These improvements enable the network to more effectively extract features at multiple scales from images and propagate them to subsequent layers. The dense connections and skip connections reduce information loss during network transmission, better preserving image details. The architectural enhancements in U-Net++ improve its generalization capability, making it more adaptable to diverse image datasets and increasing the model's versatility (Xu et al., 2021).

The high-quality label data generated via the aforementioned Wasserstein Generative Adversarial Network (WGAN), after iterative refinement, provide an extensive dataset of accurate and stable synthetic labels. These labels constitute the primary training data for the U-Net++ network. Consequently, the trained network achieves substantially enhanced accuracy, enabling precise identification of most fine fractures. Results will be presented in subsequent sections.

3 Results and discussion

3.1 Test data

The performance of current deep learning-based fracture detection methods is primarily contingent upon the quality of training samples. Model training requires large volumes of labeled data, and only datasets containing comprehensive fracture types can ensure accurate predictions. The multi-attribute fusion generative adversarial network (WGAN)-based fracture prediction method proposed in this study focuses on generating high-quality synthetic data that mirrors the quality of the input training samples, thereby significantly improving model precision. Final predictions are subsequently performed using the U-Net++ network model.

In this study, we input pre-prepared single-attribute-generated label datasets into the Wasserstein GAN for training. After network stabilization, the U-Net++ model is trained to obtain fracture prediction results. During the training process of the Wasserstein Generative Adversarial Network (WGAN), the generated dataset evolves with increasing iteration epochs. After selecting an optimal iteration count, the generated dataset undergoes normalization and is formatted into uniformly sized samples suitable for input into the U-Net++ network, thereby constructing its training dataset. This approach eliminates the labor-intensive manual annotation process while concurrently boosting the model's generalization capability.

To establish a performance benchmark, we additionally train the U-Net++ model using manually labeled datasets and Fracture interpretation results manually identified by experts (as a control

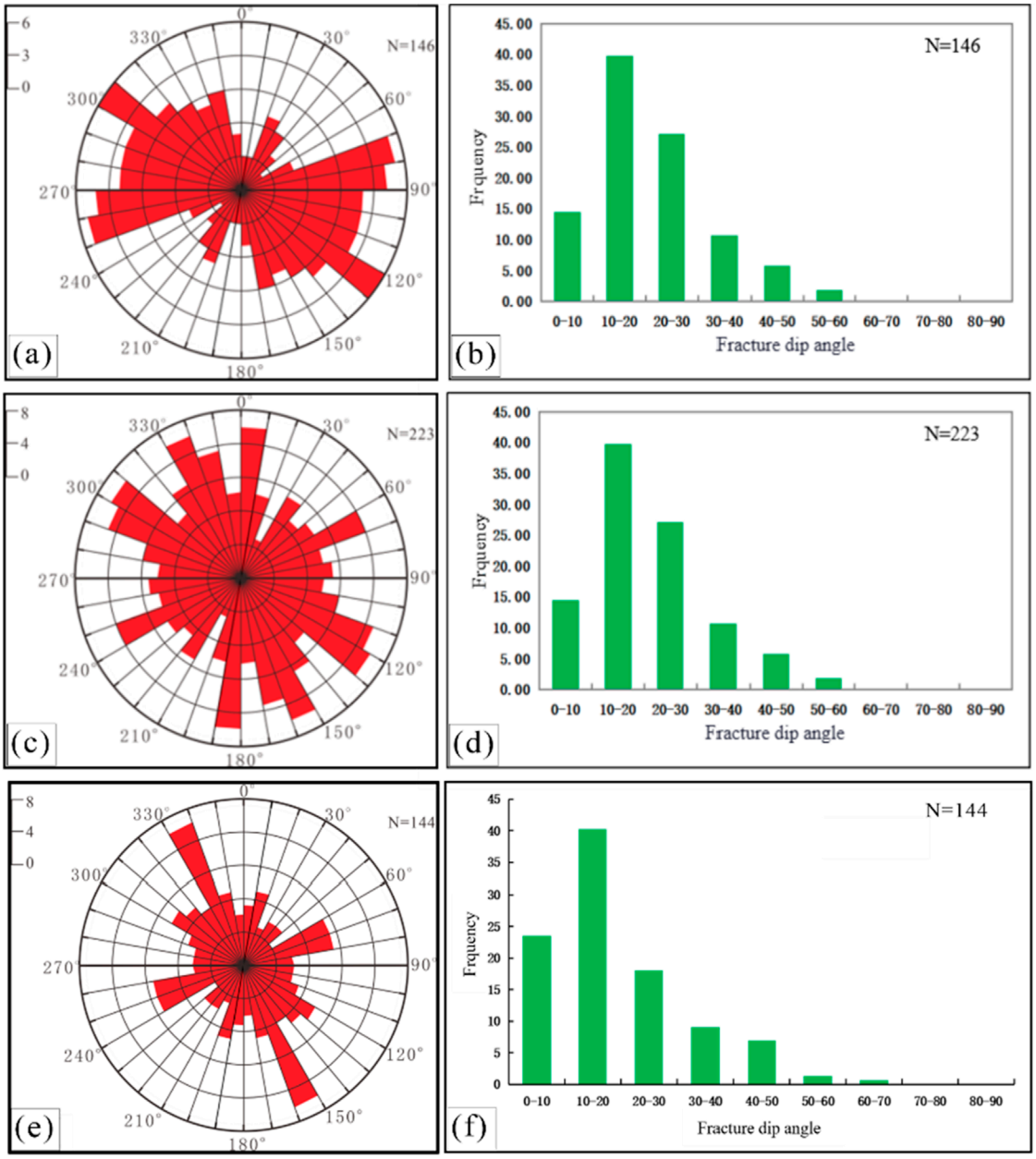

FIGURE 13
(a) Rose diagram of fracture orientations in well 1; **(b)** histogram of fracture inclination angles in well 1; **(c)** rose diagram of fracture orientations in well 2; **(d)** histogram of fracture inclination angles in well 2; **(e)** rose diagram of fracture orientations in well 3; **(f)** histogram of fracture inclination angles in well 3.

group). As shown in Figures 9–11, the proposed WGAN-based method demonstrates superior performance in identifying small fault features compared to the manual labeling approach. Given the complex structural characteristics of the study area, this advantage is particularly pronounced.

Through comparative experiments, significant differences were observed between the fracture prediction results of the U-Net++ network trained solely on manually labeled data and those trained on WGAN-augmented labeled datasets. The U-Net++ model trained with manually labeled data demonstrates the capability to effectively identify prominent faults and large fractures but exhibits limited precision in capturing subtle features, making it insufficient for comprehensive fracture characterization. In contrast, the model trained on WGAN-generated labels produces more refined and complete results. When benchmarked against manual fracture identification, our method achieves detailed characterization of small fractures. These comparative results further validate the effectiveness and practicality of the proposed approach.

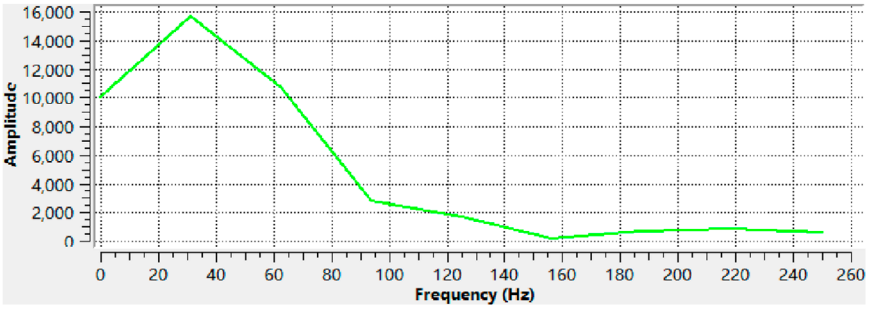

FIGURE 14
Spectral analysis of the seismic data volume.

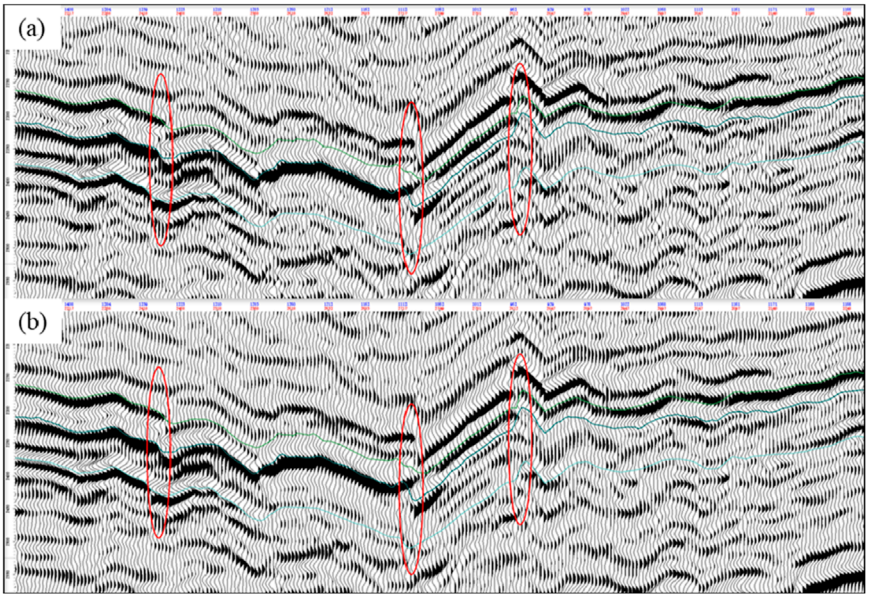

FIGURE 15
Seismic data profiles before **(a)** and after **(b)** structure-oriented filtering.

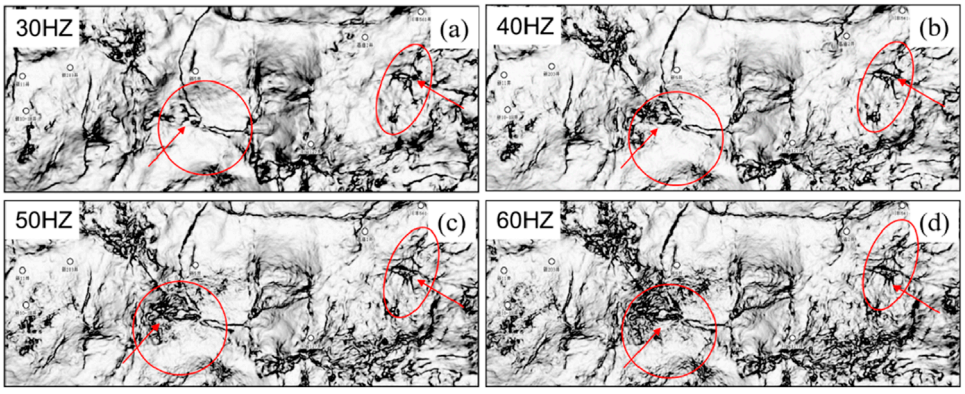

FIGURE 16
Frequency-decomposed coherence attributes based on matching pursuit. **(a)** 30 HZ, **(b)** 40 Hz, **(c)** 50 Hz, **(d)** 60 Hz.

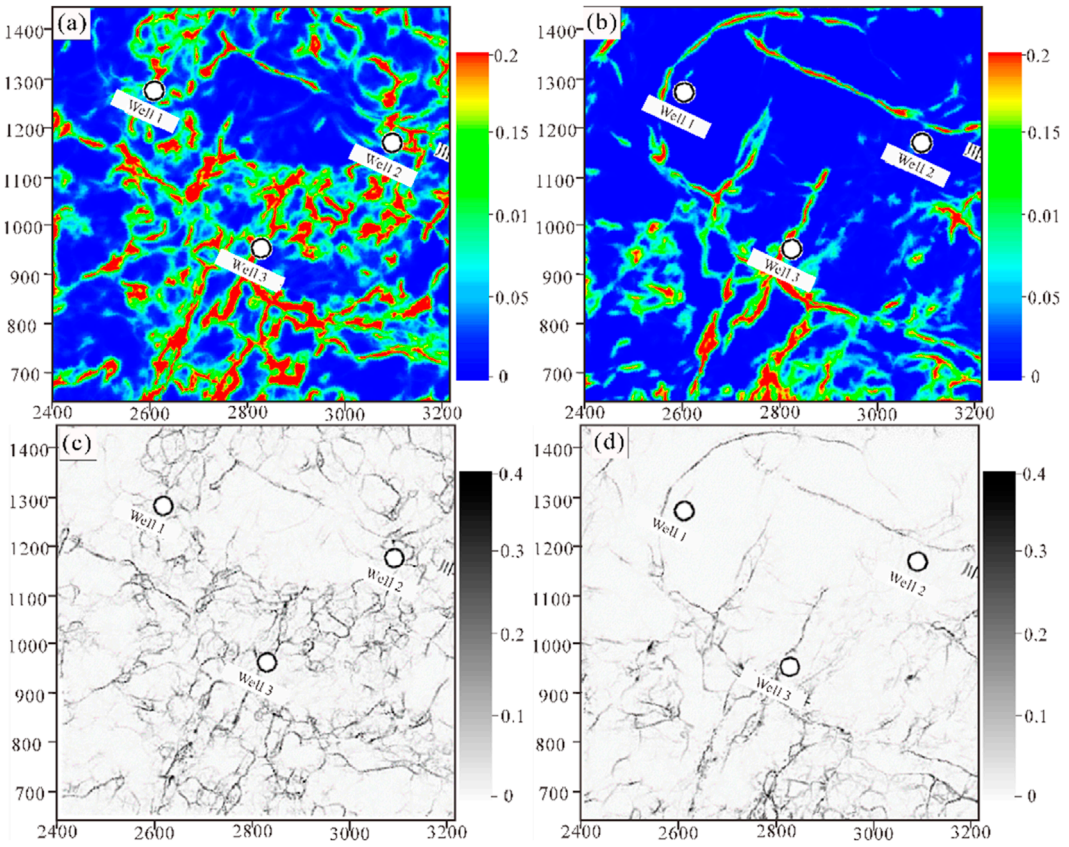

FIGURE 17
Fracture distribution based on maximum likelihood attributes for $T_3X_2^2$、$T_3X_2^4$. **(a,b)** Maximum likelihood attribute fracture distribution. **(c,d)** Refined maximum likelihood attribute fracture distribution.

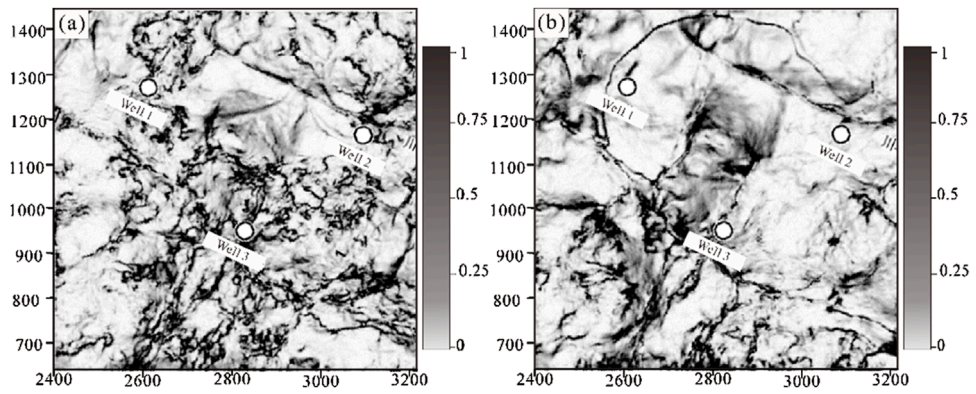

FIGURE 18
Fracture distribution based on multi-frequency coherence attribute fusion for $T_3X_2^2$ **(a)**, $T_3X_2^4$ **(b)**.

3.2 Field data

3.2.1 Study area

The study area is located in the middle-northern segment of the Western Sichuan Depression, within the Xujiahe Formation, extending in a near-east-west direction. Its boundaries are defined by the Xiaquan Structural Belt, Fenggu Structural Belt, Zitong Sag, Chengdu Sag, and its eastern margin (Wang et al., 2024). This region has undergone multiple tectonic events since the Late Triassic, forming a complex ancient large uplifted region (Deng et al., 2022; Zhao et al., 2024). The Xujiahe Formation in the Western Sichuan Depression has experienced successive tectonic movements during the Indosinian, Yanshanian, and Himalayan orogenic periods, ultimately shaping a regional structural framework characterized

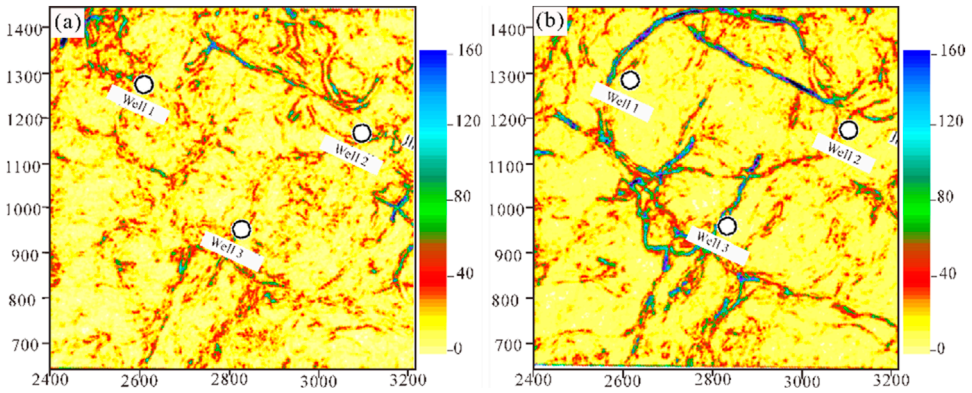

FIGURE 19
Fracture distribution based on gradient structure tensor attributes for $T_3X_2^2$ **(a)**, $T_3X_2^4$ **(b)**.

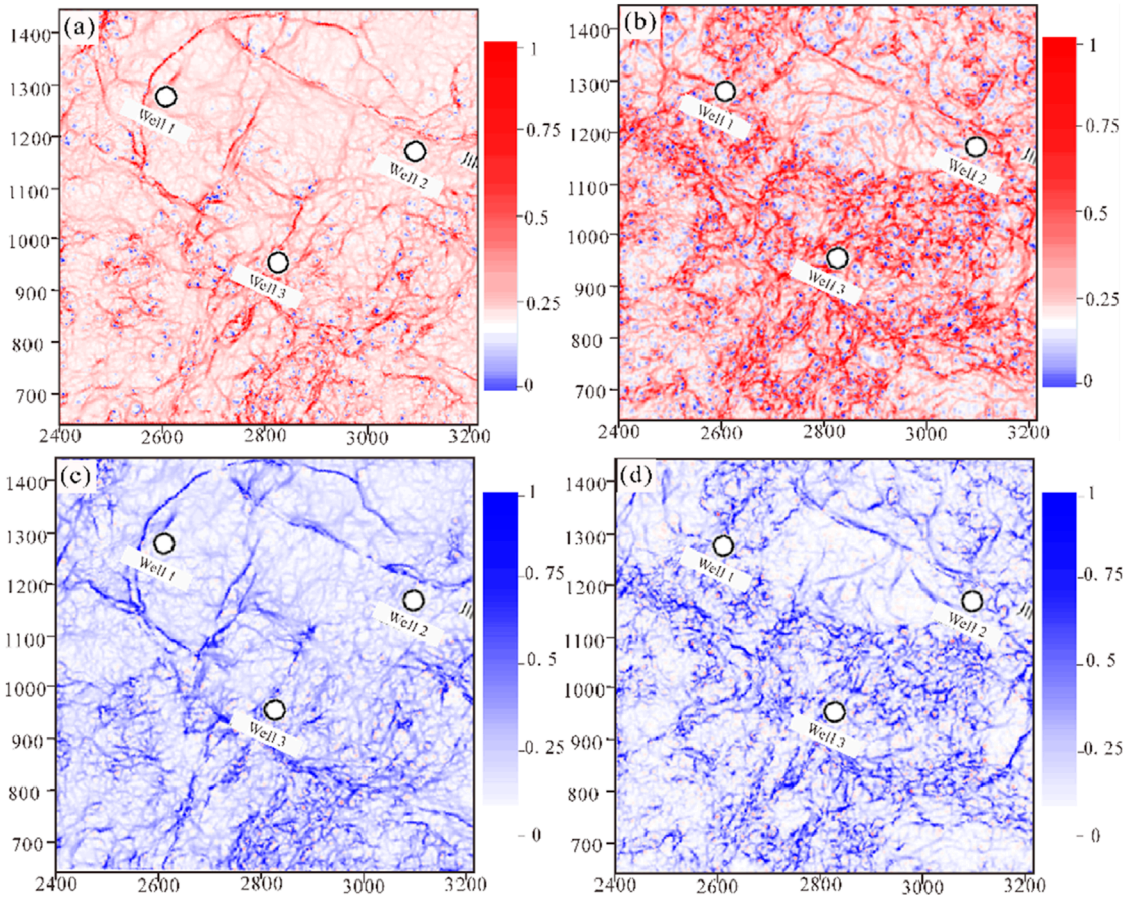

FIGURE 20
Fracture distribution based on curvature attributes for $T_3X_2^2$, $T_3X_2^4$ **(a,b)** maximum positive curvature attribute fracture distribution **(c,d)** minimum negative curvature attribute fracture distribution.

by high relief in the northwest and low-lying topography in the southeast (Zhao et al., 2017).

Well logging interpretation is essential for fracture prediction, as it provides insights into fracture development. This study primarily utilizes well logging data to conduct comparative interpretations with seismic attributes and deep learning methods, thereby verifying the accuracy of our fracture prediction results. The presence of fractures induces anomalous responses in conventional well logging curves (Figure 12), such as distinctive patterns in acoustic curves at fracture intervals. While imaging well logging offers

superior fracture identification capabilities, its high cost limits data availability in the study area. Consequently, this research combines conventional well logging data with supplementary imaging well logging data to enhance fracture identification.

Through conventional well logging and imaging well logging methods, comprehensive interpretations have been conducted to describe fracture feature variations across different regions. Below are detailed analyses of two representative wells. Figure 13 illustrates the rose diagram of fracture orientations and inclination angle distribution histogram for Well 1. The results indicate that fractures in Well one and Well three predominantly exhibit SE-NW (120°–130°) and SWW-NEE (70°–90°) orientations. Fracture inclinations are primarily 0°–10°, with moderate-to-high-angle fractures (10°–30°) also well-developed. Additionally, fracture aperture increases progressively with depth. Figure 13 displays the rose diagram and inclination angle distribution histogram for Well 2. Fractures in this well are dominated by low-angle orientations (10°–20°), while moderate-angle fractures are underdeveloped, and high-angle fractures are absent. In the Xu2 Member, fracture linear density initially increases with depth and then fluctuates downward.

Based on calculating the linear density of fractures in the target stratigraphic interval (Xu2 Member of the Xujiahe Formation), high-value zones of fracture density are identified within the three-stage tectonic stress integration region. The well logging results will serve as the primary validation basis for subsequent fracture prediction outcomes derived from multi-attribute prediction and the multi-attribute fusion generative adversarial network (WGAN) method. Through integration with well logging interpretations and fracture development characteristics, the final fracture characterization results will achieve greater credibility.

3.2.2 Conventional attribute-based fracture prediction

Seismic data with distinct attribute characteristics play a crucial role in fracture identification. The Xujiahe Formation primarily consists of tight sandstone deposits, and its seismic data exhibit high quality, with notable resolution and frequency attributes. As shown in Figure 14, the seismic bandwidth is 63 Hz, and spectral analysis reveals that the dominant frequencies are primarily distributed between 20 Hz and 80 Hz.

The identification results of fractures vary under different frequency characteristics. In this study, we employ Matching Pursuit Spectral Decomposition (MPSD) processing within the effective frequency band to obtain distinct frequency-component volumes. Subsequently, structure-oriented filtering is applied to these frequency volumes to enhance the detectability of fault dip strength and azimuth attributes (Figure 15). This integrated approach yields results that more accurately characterize fracture features, as the frequency-dependent processing better captures fracture-related seismic responses while structural filtering improves the continuity and interpretability of fracture systems. The methodology demonstrates superior performance in identifying multi-scale fractures compared to conventional full-spectrum approaches, particularly in complex tight sandstone reservoirs where fracture manifestations vary significantly across frequency bands.

As illustrated in Figure 16, this study selects frequency-component volumes at 30 Hz, 40 Hz, 50 Hz, and 60 Hz for coherence attribute processing, yielding distinct fracture identification outcomes.

As shown in the figure above, different frequency bands exhibit distinct responses to fractures of varying scales. Coherence processing of low-frequency components can effectively characterize medium-to-large scale fractures, while coherence processing of high-frequency components can delineate small-scale fractures and fractures zones (Bahorich and Farmer, 1995). Through coherence slices at different scales, it can be observed that low-frequency components mainly reflect the macro-scale distribution of fracture development, whereas high-frequency components can provide more detailed characterization of small-scale fractures (Gersztenkorn and Marfurt, 2002).

To evaluate the method proposed in this study, we performed additional fracture identification using four attributes (Huang et al., 2025). The specific results are shown below (All the result values in the figure are obtained after standardized processing using this method (Niu et al., 2025; Ren et al., 2024). The larger the value, the greater the probability of fracture distribution (Li et al., 2024; Zhang et al., 2025).

Fracture prediction based on maximum likelihood attributes demonstrates that both standard and refined maximum likelihood approaches achieve comprehensive delineation of large fractures. Particularly noteworthy is that the refined maximum likelihood method enhances the identification of small fractures (Figure 17).

The fundamental principle of fracture prediction based on coherence attributes lies in delineating fractures by analyzing lateral variations in seismic waveform continuity. This method enables clear identification of large-scale fractures within the seismic dataset (Figure 18; Kurt et al., 2012).

Compared with coherence attributes and maximum likelihood attributes, the fracture layering description derived from gradient structure tensor attributes provides clearer delineation of fracture angles and large-scale structural features (Chen et al., 2012). However, it exhibits limitations in characterizing small fractures (Wang et al., 2018). In essence, this approach yields more accurate information on the overall fracture trends within the Xujiahe Formation (Figure 19; Chopra and Marfurt, 2007; Lou et al., 2022).

Fracture prediction based on curvature attributes exhibits a strong response to linear features, enabling clear characterization of fault structures and fracture delineation. Among the commonly used methods, maximum positive curvature and minimum negative curvature attributes yield the most effective results (Roberts, 2001). The curvature calculations of both approaches enhance the description of stratal bending, produce stronger responses at fracture locations, and provide richer geometric information about the formations (Figure 20; Suo et al., 2012).

TABLE 1 Neural network architecture and hyperparameters.

Parameter	Value
Epochs	500
Initial Learning Rate	0.005
Batch Size	5
LeakyReLU	0.2

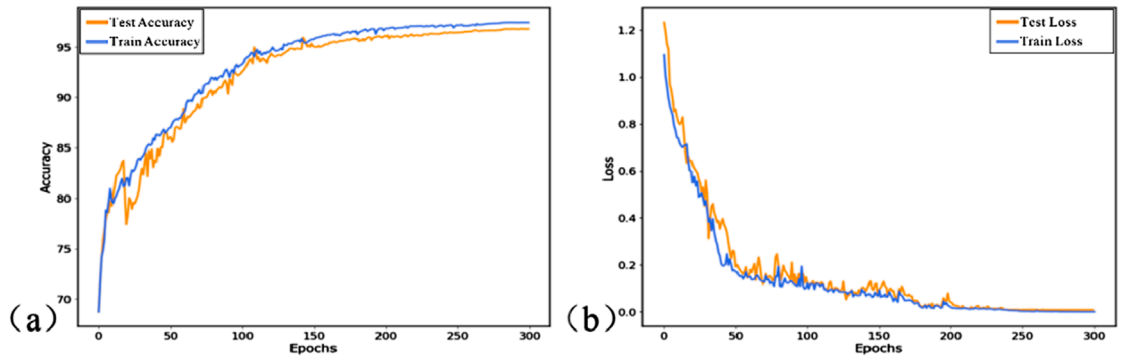

FIGURE 21
(a) U-Net++ accuracy curve; **(b)** U-Net++ loss curve.

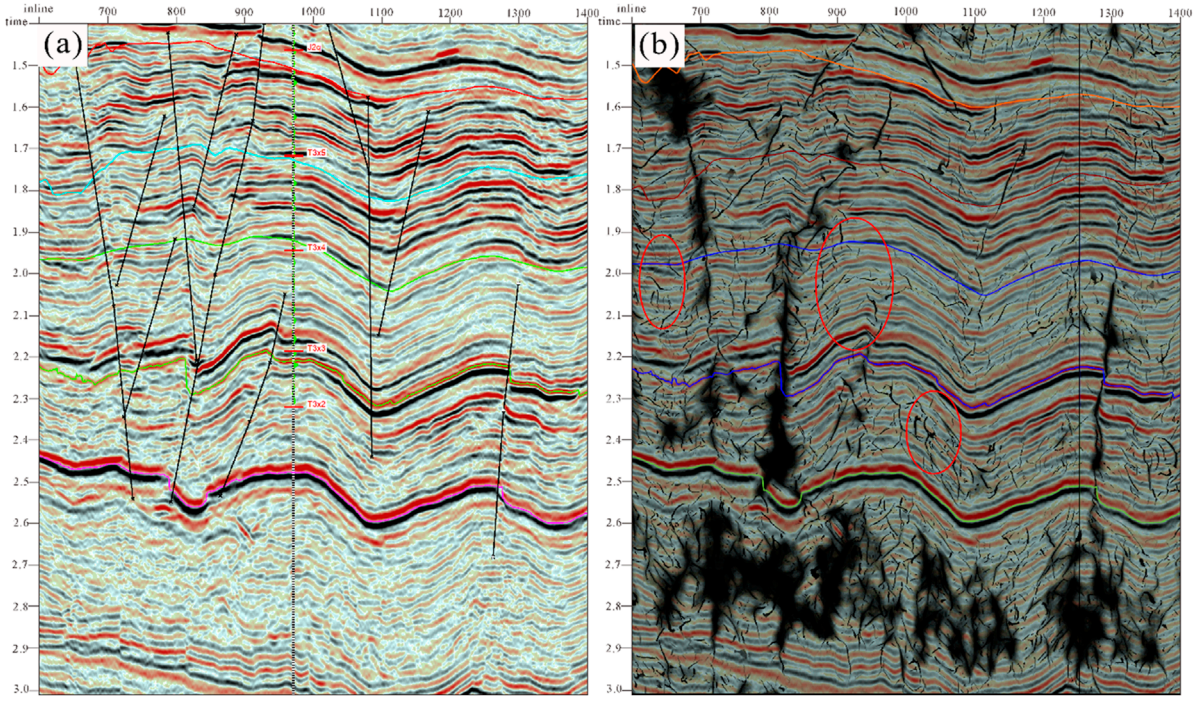

FIGURE 22
Comparison of manual interpretation **(a)** and multi-attribute fusion generative adversarial network model identification results **(b)** (Crossline = 2,830).

3.3 Fracture prediction results using the multi-attribute fusion generative adversarial network

Since the prediction results of seismic data attributes (e.g., maximum likelihood attributes, coherence attributes, gradient structure tensor attributes, and curvature attributes) exhibit higher authenticity compared to manually labeled data, the labels generated by the Wasserstein generative adversarial network (WGAN) can serve as reliable ground-truth labels for real seismic data (Kosters et al., 2008). After further optimization through the U-Net++ network architecture, the predicted results achieve significantly improved geological authenticity and reliability.

The model parameters are configured as Table 1, the stochastic gradient descent (SGD) algorithm is selected as the optimizer with an initial learning rate of 0.005, which is reduced by half every 50 epochs. The discriminator network employs a LeakyReLU activation function with the negative slope parameter set to 0.2.

Building on the multi-attribute analysis results in this chapter, we input all single-attribute fracture prediction results into the Wasserstein Generative Adversarial Network (WGAN) to generate and augment synthetic data, thereby addressing the insufficiency of conventional network datasets. The network is optimized by adjusting parameters such as loss rate and accuracy. Once stabilized, the synthetic data stored in the WGAN generator is extracted and integrated with multi-attribute fracture

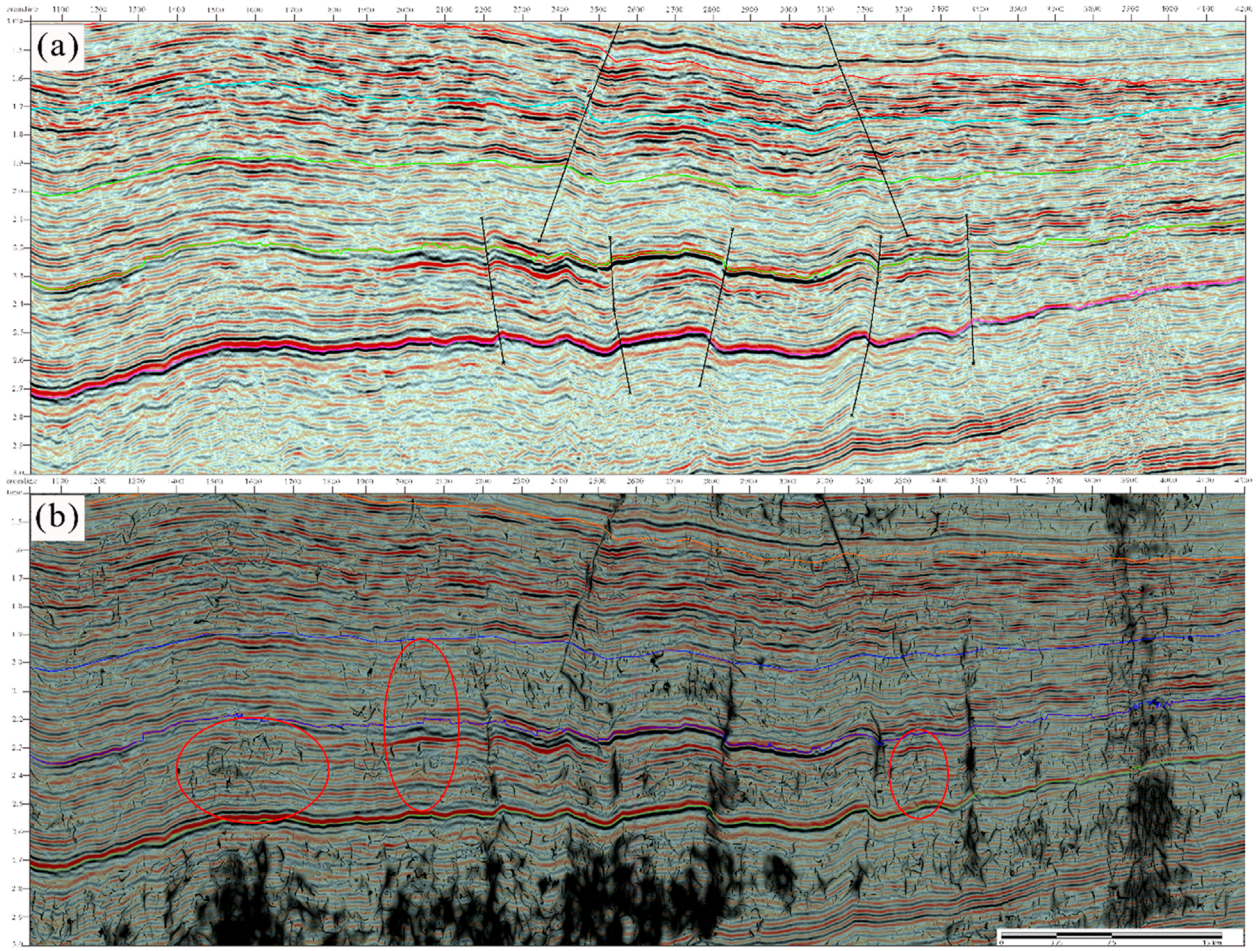

FIGURE 23
Comparison of manual interpretation **(a)** and multi-attribute fusion generative adversarial network model identification results **(b)** (inline = 1,290).

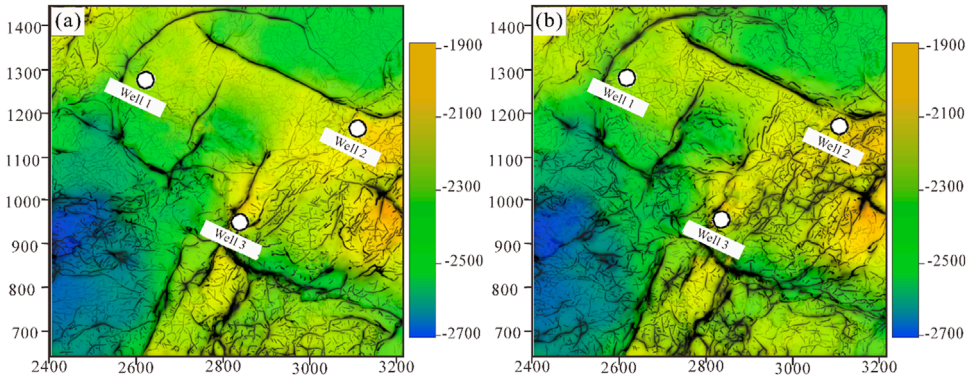

FIGURE 24
$T_3X_2^2$ **(a)**, $T_3X_2^4$ **(b)** fracture-structure overlay map.

identification results to train the U-Net++ network for fracture prediction.

The U-Net++ network was trained using a dataset comprising 180 samples, including 150 training datasets and 30 testing datasets. The curves of loss rate and accuracy during training are presented in Figure 21.

Figures 22, 23 present integrated results of fracture prediction via the multi-attribute fusion generative adversarial network

(WGAN) fused with seismic cross-sections. Extracted cross-sectional data from xline = 2,800 and inline = 1,390 are benchmarked against human-expert fault interpretations. The predicted fractures, including major discontinuities corroborated by field operations, exhibit substantial concordance with expert interpretations. Notably, the WGAN framework demonstrates enhanced resolution of minor fractures, effectively identifying fine-scale fractures that are challenging for conventional manual methods. Validation via well log interpretations and multi-attribute prediction benchmarks confirms the method's robust accuracy and adaptability in fracture characterization.

To better visualize fractures in the Xujiahe Formation, we performed stratigraphic slicing on the final results and overlaid them with structural maps to demonstrate fracture distribution (Figure 24). The structural-fracture overlay analysis reveals that neural network mapping effectively resolves both the overall morphology and internal details of fractures, confirming the accuracy and reliability of the proposed method. Planar views derived from the slices clearly delineate fracture networks, providing precise spatial characterization within the study area. Furthermore, profile views align predicted fractures with actual drilling data, offering additional validation of the method's robustness in capturing subsurface fracture systems.

4 Conclusion

This study proposes a fracture prediction method based on a multi-attribute fusion generative adversarial network (WGAN-U-Net++). By integrating multi-attribute prediction results, the approach first employs the Wasserstein generative adversarial network (WGAN) to generate augmented samples, followed by the U-Net++ network to achieve high-resolution fracture characterization in the Xujiahe Formation. Experimental results demonstrate that this method outperforms traditional approaches and well-log data in both profile and slice interpretations, enabling precise delineation of complex fracture networks.

Focusing on the tight sandstone reservoirs of the Xujiahe Formation in the Western Sichuan Foreland Basin (characterized by continental deposition and multiphase tectonic superposition), this research addresses the application of deep learning in fracture identification. The study area exhibits complex fracture systems and weakened distribution patterns due to multiphase tectonic activities, coupled with strong heterogeneity in sedimentary environments and hydrocarbon accumulation conditions, rendering conventional methods ineffective for high-precision prediction. To tackle the challenge of deep learning's reliance on high-quality labeled datasets, the proposed WGAN-U-Net++ framework integrates multi-attribute fusion and sample augmentation, thereby significantly improving the reliability of fracture identification in tight sandstones. This framework presents a novel approach for fracture prediction in complex geological settings.

Data availability statement

The original contributions presented in the study are included in the article/supplementary material, further inquiries can be directed to the corresponding author.

Author contributions

YZ: Conceptualization, Writing – original draft, Investigation, Methodology, Writing – review and editing, Data curation. XW: Funding acquisition, Conceptualization, Supervision, Writing – review and editing. YL: Writing – original draft, Methodology, Validation. XJ: Conceptualization, Writing – review and editing. HZ: Validation, Formal Analysis, Writing – original draft.

Funding

The author(s) declare that financial support was received for the research and/or publication of this article. This paper is supported by National Natural Science Foundation of China (Grant No. 42074163).

Conflict of interest

The authors declare that the research was conducted in the absence of any commercial or financial relationships that could be construed as a potential conflict of interest.

Generative AI statement

The author(s) declare that no Generative AI was used in the creation of this manuscript.

Any alternative text (alt text) provided alongside figures in this article has been generated by Frontiers with the support of artificial intelligence and reasonable efforts have been made to ensure accuracy, including review by the authors wherever possible. If you identify any issues, please contact us.

Publisher's note

References

Bahorich, M., and Farmer, S. (1995). 3-D seismic discontinuity for faults and stratigraphic features: the coherence cube. *Lead. Edge* 14 (10), 1053–1058. doi:10.1190/1.1437077

Bhunia, A. K., Banerjee, P., Konwer, A., Bhowmick, A., Roy, P. P., Pal, U., et al. (2018). "Word level font-to-font imagetranslation using convolutional recurrent generative adversarial networks," in *24th international conference*

on pattern recognition (ICPR), 2018, 3645–3650. doi:10.1109/ICPR.2018.8545184

Bi, Z., and Wu, X. (2021). Improving fault surface construction with inversion-based methods. *Geophysics* 86 (1), IM1–IM14. doi:10.1190/geo2019-0832.1

Cai, J., Ding, S., Zhang, Q., Liu, R., Zeng, D., and Zhou, L. (2022). Broken ice circumferential crack estimation *via* image techniques. *Ocean. Eng.* 259, 111735. doi:10.1016/j.oceaneng.2022.111735

Cao, D., Zeng, L., Gomez-Rivas, E., Gong, L., Liu, G., Bons, P. D., et al. (2024). Correction of linear fracture density and error analysis using underground borehole data. *J. Struct. Geol.* 184, 105152. doi:10.1016/j.jsg.2024.105152

Chan, S., Huang, C., Bai, C., Ding, W., and Chen, S. (2022). Res2-UNeXt: a novel deep learning framework for few-shot cell image segmentation. *Multimedia Tools Appl.* 81 (10), 13275–13288. doi:10.1007/s11042-021-10536-5

Chen, X., Yang, W., He, Z., Zhong, W. L., and Wen, X. T. (2012). The algorithm of 3D multi-scale volumetric curvature and its application. *Appl. Geophys.* 9 (1), 65–72. doi:10.1007/s11770-012-0315-7

Chopra, S., and Arfut, K. J. (2010). Ntegration of coherence and volumetric curvature images i. *Lead. Edge* 29 (9), 1092–1107. doi:10.1190/1.3485769

Chopra, S., and Marfurt, K. J. (2007). Seismic attributes for prospect identification and Reservoir characterization. *Society of Exploration Geophysicists*, 10 (11), 457–464.

Chopra, S., and Marfurt, K. J. (2007). *Seismic attributes for prospect identification and Reservoir characterization*. Society of Exploration Geophysicists.

Cui, X., Liu, Y., Du, X., Xiao, H., Xu, H., and Du, Y. (2025). Effect of fault dislocation on the deformation and damage behavior of ballastless track structures in tunnels. *Transp. Geotech.* 52, 101561. doi:10.1016/j.trgeo.2025.101561

Deng, J., Liu, M., Ji, Y., Tang, D., Zeng, Q., Song, L., et al. (2022). Controlling factors of tight sandstone gas accumulation and enrichment in the slope zone of foreland basins: the Upper Triassic Xujiahe Formation in Western Sichuan Foreland Basin, China. *J. Petroleum Sci. Eng.* 214, 110474. 0920-4105. doi:10.1016/j.petrol.2022.110474

Di, H., Zhao, T., Vikram, J., Wu, X., Huang, L., AlRegib, G., et al. (2019). Introduction to special section: machine learning in seismic data analysis. *Interpretation* 7 (3), T351–T359. doi:10.1190/int-2019-0609-spseintro.1

Ding, C., Guo, X., Xiao, C., Sui, Z., and Yang, Y. (2025). Experimental Study on the influence of blast hole bottom cushion medium on blasting damage characteristics and strain evolution of rock mass. *Rock Mech. Rock Eng.* 58 (2), 1895–1909. doi:10.1007/s00603-024-04276-9

Dorigo, M., Caro, G. D., and Gambardella, M. L. (1999). Ant algorithms for discrete optimization. *Artif. Life* 5 (2), 137–172, April. doi:10.1162/106454699568728

Fu, L., Guo, J., Shen, W., Wang, X., Liu, X., Chen, X., et al. (2024). Geophysical evidence of the collisional suture zone in the prydz Bay, East Antarctica. *Geophys. Res. Lett.* 51 (2), e2023GL106229. doi:10.1029/2023GL106229

Gan, B., Li, Z., Huo, W., Zhang, Y., Li, Z., Fan, R., et al. (2025). Phase transitions of CH4 hydrates in mud-bearing sediments with oceanic laminar distribution: mechanical response and stabilization-type evolution. *Fuel* 380, 133185. doi:10.1016/j.fuel.2024.133185

Gersztenkorn, A., and Marfurt, K. J. (2002). Eigenstructure-based coherence computations as an aid to 3-D structural and stratigraphic mapping. *Geophysics* 64 (5), 1468–1479. doi:10.1190/1.1444651

Gibson, D., Spann, M., and Turner, J. (2003). *Automatic fault detection for 3D seismic Data[C]//DICTA*, 821–830.

Höcker, C., and Fehmers, G. (2002). Fast structural interpretation with structure-oriented filtering. *Lead. Edge* 21 (3), 238–243. doi:10.1190/1.1463775

Huang, L., Guan, W., Guan, Y., Zhao, H., Zhang, Z., and Wen, Y. (2025). Overburden movement law in strip filling mining of upward mining faces. *Sci. Rep.* 15 (1), 1378. doi:10.1038/s41598-024-82930-6

Kingma, D. P., and Ba, J. (2014). Adam: a method for stochastic optimization. *Comput. ence. CoRR, abs/1412.6980*.

Kosters, M., Hague, P. F., Hofmann, R. A., and Hughes, B. (2008). "Integrated modeling of karstification of a Central Luconia Field Sarawak[C]," *Paper presented at the International Petroleum Technology Conference* (Kuala Lumpur, Malaysia), 3–5. doi:10.2523/IPTC-12327-MS

Kurt, J., Marfurt, R., Lynn, K., and Steven, L. (2012). 3-D seismic attributes using a semblance-based coherency algorithm. *Geophysics* 63 (4), P1150–P1165. doi:10.1190/1.144415

Lecun, Y., Bottou, L., Bengio, Y., and Haffner, P. (1998). Gradient-based learning applied to document recognition. *Proc. IEEE* 86 (11), 2278–2324. doi:10.1109/5.726791

Ledig, C., Theis, L., Huszar, F., Caballero, J., Cunningham, A., Acosta, A., et al. (2017). "Photo-realistic single image super-resolution using a generative adversarial network[C]," in *The lEEE conference on computer vision and pattern recognition (CVPR)*. doi:10.48550/arXiv.1609.04802

Lei, J., Fang, H., Zhu, Y., Chen, Z., Wang, X., Xue, B., et al. (2024). GPR detection localization of underground structures based on deep learning and reverse time migration. *NDT and E Int.* 143, 103043. doi:10.1016/j.ndteint.2024.103043

Li, Y., Jia, D., Wang, S., Qu, R., Qiao, M., and Liu, H. (2024). Surrogate model for reservoir performance prediction with time-varying well control based on depth generative network. *Petroleum Explor. Dev.* 51 (5), 1287–1300. doi:10.1016/S1876-3804(25)60541-6

Li, L., Jin, H., Tu, W., and Zhou, Z. (2024). Study on the minimum safe thickness of water inrush prevention in karst tunnel under the coupling effect of blasting power and water pressure. *Tunn. Undergr. Space Technol.* 153, 105994. doi:10.1016/j.tust.2024.105994

Liu, G., Kang, J., Zhong, Z., Bo, W., Fan, H., and Yang, C. (2025). Laboratory experiments and 3D DDA Numerical simulations on rockfall movement characteristics. *Rock Mech. Rock Eng.* 58 (8), 9747–9769. doi:10.1007/s00603-025-04648-9

Liu, Z., Song, C., Cai, H., Yao, X., and Hu, G. (2017). Enhanced coherence using principal component analysis. *Interpretation* 5(3), T351–T359. doi:10.1190/int-2016-0194.1

Lou, Y., Zhang, H., Liu, N., Liu, R., and Sun, F. (2022). Multiscale coherence attribute and its application on seismic discontinuity description. *IEEE Geoscience Remote Sens. Lett.* 19, 1–5. doi:10.1109/LGRS.2021.3132358

Mao, X., Li, Q., Xie, H., Lau, R. Y. K., Wang, Z., and Smolley, S. P. (2017). "Least squares generative adversarial networks[C]," in *Proceedings of the IEEE international conference on computer vision and pattern recognition*, 2794–2802. doi:10.48550/arXiv.1611.04076

Marfurt, K. J., Kirlin, R. L., Farmer, S. L., and Bahorich, M. S. (1998). 3D seismic attributes using a semblance-based coherency algorithm. *Geophysics* 63 (04), 1150–1165. doi:10.1190/1.1444415

Niu, Q., Hu, M., Chang, J., Wang, W., Yuan, W., Wang, Q., et al. (2024). Explosive fracturing mechanism in low-permeability sandstone-type uranium deposits considering different acidification reactions. *Energy* 312, 133676. doi:10.1016/j.energy.2024.133676

Niu, Q., Zhao, X., Chang, J., Qi, X., Shangguan, S., Wang, W., et al. (2025). Numerical simulation on physical composite stimulation and geothermal development performance of hot dry rock: a case study from Matouying Uplift, China. *Appl. Therm. Eng.* 267, 125714. doi:10.1016/j.applthermaleng.2025.125714

Ren, Q., Li, L., Wang, J., Jiang, R., Li, M., and Feng, J. W. (2024). Dynamic evolution mechanism of the fracturing fracture system—Enlightenments from hydraulic fracturing physical experiments and finite element numerical simulation. *Petroleum Sci.* 21 (6), 3839–3866. doi:10.1016/j.petsci.2024.09.004

Roberts, A. (2001). Curvature attributes and their application to 3D interpreted horizons. *First Break* 19, 85–100. doi:10.1046/j.0263-5046.2001.00142.x

Sun, H., Wang, Y., Jia, L., Lin, Z., and Yu, H. (2024). Theoretical and numerical methods for predicting the structural stiffness of unbonded flexible riser for deep-sea mining under axial tension and internal pressure. *Ocean. Eng.* 310, 118672. doi:10.1016/j.oceaneng.2024.118672

Suo, C., Peng, S., Chang, S., Duan, R., and Wang, G. (2012). A new calculating method of the curvature to predicting the Reservoir fractures. *Procedia Environ. Sci.* 12, 576–582. doi:10.1016/j.proenv.2012.01.320

Wang, S., Yuan, S., Wang, T., Gao, J., and Li, S. (2018). Three-dimensional geosteering coherence attributes for deep-formation discontinuity detection. *Geophysics* 83 (6), O105–O113. doi:10.1190/geo2017-0642.1

Wang, A., Liu, J., Liu, Z., Xiao, K., Huang, Y., Fan, L., et al. (2024). Genetic mechanisms of high-quality tight siliciclastic reservoirs: a case study from the Upper Triassic Xujiahe Formation in the Yuanba area, Sichuan Basin, China. *Energy Geosci.* 5, 100290. doi:10.1016/j.engeos.2024.100290

Wu, X., and Dave, H. (2016). 3D seismic image processing for faults. *Geophysics* 81 (2), IM1–IM11. doi:10.1190/geo2015-0380.1

Wu, Y., Shuai, H., Tam, Z., and Chiu, H. (2021). "Gradient normalization for generative adversarial networks[C]," in *Proceedings of the IEEE/CVF international conference on computer vision*, 6373–6382. doi:10.48550/arXiv.2109.02235

Xu, W., Long, C., Wang, R., and Wang, G. (2021). "DRB-GAN: a dynamic resblock generative adversarial network for artistic style transfer[C]," in *Proceedings of the IEEE/CVF international conference on Computer Vision*, 6383–6392. doi:10.48550/arXiv.2108.07379

Xu, D., Jiang, L., Qin, Y., Shen, H., and Ji, B. (2024). High-precision FBG-based sensor for soil settlement monitoring: a comparative study with magnetic settlement gauges and PIV technique. *Sensors Actuators A Phys.* 366, 114935. doi:10.1016/j.sna.2023.114935

Xue, Y., Chang, F., Zhang, D., and Chen, Y. (2016). Simultaneous sources separation *via* an iterative rank-increasing method. *IEEE Geoscience Remote Sens. Lett.* 13 (12), 1915–1919. doi:10.1109/lgrs.2016.2617338

Yongshi, W., Yang, G., and Zhengwei, F. (2021). Pore throat structure and classification of Paleogene tight reservoirs in jiyang depression, Bohai Bay Basin, China. *Petroleum Explor. Dev. Online* 48(2), 308–322. doi:10.1016/s1876-3804(21)60025-3

Yuan, Y., Qin, G., Li, D., Zhong, M., Shen, Y., and Ouyang, Y. (2024). Real-Time joint filtering of gravity and gravity gradient data based on improved kalman filter. *IEEE Trans. Geoscience Remote Sens.* 62, 1–12. doi:10.1109/TGRS.2024.3452038

Zhang, H., Bao, X., Zhao, H., Hao, Y., Huang, H., Dai, M., et al. (2025). High-Precision deblending of 3-D simultaneous source data based on prior information constraint. *IEEE Geoscience Remote Sens. Lett.* 22, 1–5. doi:10.1109/LGRS.2025.3526972

Zhang, C., Zhu, Z., Dai, L., Wang, S., and Shi, C. (2025). The incompatible deformation mechanism of underground tunnels crossing fault conditions in the southwest edge strong seismic zone of the Qinghai-Tibet Plateau: a study of shaking table test. *Soil Dyn. Earthq. Eng.* 197, 109482. doi:10.1016/j.soildyn.2025.109482

Zhao, H., Shi, J., Qi, X., Wang, X., and Jia, J. (2017). "Pyramid scene parsing network [C]," in *Proceedings of the IEEE conference on computer vision and pattern recognition (CVPR).* Honolulu, HI: United States, 2881–2890. doi:10.1109/CVPR.2017.660

Zhao, Y., Huang, G., Liang, Q., and Chen, Q. (2024). Study on microscopic characteristics and rock mechanical properties of tight sandstone after acidification–supercritical CO2 composite action: case study from Xujiahe Formation, China. *Appl.* 14, 4108. doi:10.3390/app14104108

Zhou, G., Wang, Z., and Li, Q. (2022). Spatial negative co-location pattern directional mining algorithm with join-based prevalence. *Remote Sens.* 14 (9), 2103. doi:10.3390/rs14092103

Zhu, Y., Park, T., Isola, P., and Efros, A. A. (2017). "Unpaired image-to-image translation using cycle-consistentadversarial networks, " in *2017 IEEE International Conference on Computer Vision ICCV*, 2242–2251. doi:10.1109/ICCV.2017.244